Numerical computation of the hypersonic leading edge problem using the Burnett equations

John C. Tannehill and Gerald R. Eisler

Citation: Physics of Fluids **19**, 9 (1976); doi: 10.1063/1.861304
View online: http://dx.doi.org/10.1063/1.861304
View Table of Contents: http://scitation.aip.org/content/aip/journal/pof1/19/1?ver=pdfcov
Published by the AIP Publishing

Numerical computation of the hypersonic leading edge problem using the Burnett equations

John C. Tannehill and Gerald R. Eisler*

Department of Aerospace Engineering and Engineering Research Institute, Iowa State University, Ames, Iowa 50010

(Received 6 February 1975; final manuscript received 28 July 1975)

The hypersonic rarefied flow near the sharp leading edge of a flat plate is computed for the first time using a finite-difference solution of the complete, unsteady Burnett equations. The computation is advanced in time from the initial conditions until the steady-state solution is reached. The computational region extends from the leading edge to the strong-interaction regime. Schamberg's second-order wall slip and temperature jump boundary conditions are employed at the wall. The numerical results are compared with experimental data, a Monte Carlo simulation, and a finite-difference solution of the complete Navier–Stokes equations. Based on these comparisons, it is evident that the Burnett equations in conjunction with Schamberg's second-order boundary conditions give a much less accurate description of the rarefied flow field near the leading edge than do the Navier–Stokes equations.

I. INTRODUCTION

The hypersonic leading edge problem has been the subject of a considerable number of both experimental and theoretical investigations over the past two decades. A flow model[1] which has evolved from these studies is shown in Fig. 1. At the leading edge, the mean-free-path of the molecules is very large, and the frequency of collisions with the flat plate dominates over the frequency of collisions between molecules. This flow is a near free-molecule flow and can be described only on the basis of kinetic theory. A transition region with mixed kinetic and continuum properties exists between the near free-molecule region and the merged-layer region. In the merged-layer region, the shock wave and viscous layer are still fully merged and indistinguishable from each other. Many believe that the flow in this region can be described by the equations of continuum mechanics if velocity slip and temperature jump are accounted for at the wall. The downstream limit of the merged layer is reached when a distinct inviscid layer develops between the shock wave and the viscous layer. This is the beginning of the interaction region which has been further divided into the strong- and weak-interaction regions. The weak-interaction region eventually evolves into the classical Prandtl boundary layer flow far downstream.

The theoretical investigations which have been conducted to solve the leading edge flow field can be divided into two groups, depending on whether a kinetic theory approach or a continuum flow approach is used. Included in the first approach are the Monte Carlo simulation method[2] and the technique of solving the Boltzmann equation using the Bhatnagar–Gross–Krook approximation model.[3]

In the continuum approach, the problem has, until recently, been solved using various simplifications of the complete Navier–Stokes equations. Several studies[4,5] have used the concept of "local similarity" in both the viscous layer and the shock layer to reduce the Navier–Stokes equations to ordinary differential equations. Later investigations[6,7] have used the thin-layer approximation to reduce the Navier–Stokes equations to a set of parabolic equations which can be solved using standard boundary layer techniques. These equations are valid in the merged-layer and strong-interaction regions, but they fail to provide an adequate solution at the leading edge where the neglected streamwise gradient terms become significant. Recently, solutions for the leading edge problem using the complete Navier–

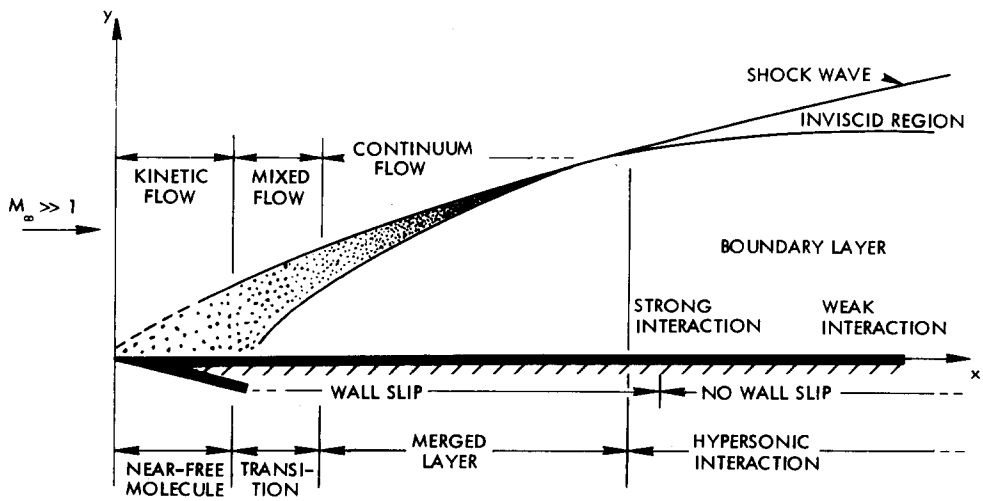

FIG. 1. Hypersonic rarefied flow past a sharp leading-edge plate.

Stokes equations have been made by Butler[8] using the fluid-in-cell and particle-in-cell methods and simultaneously by Cheng and Chen[9] and Tannehill *et al.*[10] using finite-difference methods. These studies have shown surprisingly good agreement with kinetic theory results even though the Navier–Stokes equations are strictly valid for continuum flows only. In addition to these flat plate studies, several investigators[11,12] have recently used the complete Navier–Stokes equations to solve blunt-body rarefied flow fields, and their results agree very well with previous Monte Carlo calculations.

In the present study, the rarefied flow near the sharp leading edge of a flat plate is computed for the first time, using the complete Burnett equations. The Burnett equations are a higher order set of equations (in terms of the Knudsen number) than the Navier–Stokes equations, and thus it might be reasonable to assume that they would yield better results than the Navier–Stokes equations in rarefied flow regions. However, Kogan[13] has stated that while the Burnett equations can be used to improve the solution in regions where the Navier–Stokes equations have good accuracy, it is not safe to assume that they can be used to progress into more rarefied regions where the Navier–Stokes equations are already unsuitable. In view of the recent success of using the complete Navier–Stokes equations to solve selected rarefied flow problems, it is not entirely clear whether the Burnett equations would or would not provide a more accurate description of the leading edge flow field. The present study was undertaken to explore this possibility.

II. GOVERNING EQUATIONS

The conservation equations for a two-dimensional, unsteady, nonreacting flow without body forces or external heat additions can be written in divergence vector form as

$$\frac{\partial \mathbf{U}}{\partial t}+\frac{\partial \mathbf{F}}{\partial x}+\frac{\partial \mathbf{G}}{\partial y}=0\,, \tag{1}$$

where

$$\mathbf{U}=\begin{bmatrix}\rho\\ \rho u\\ \rho v\\ E\end{bmatrix},\quad \mathbf{F}=\begin{bmatrix}\rho u\\ \rho u^2+p-\tau_{xx}\\ \rho uv-\tau_{xy}\\ Eu+pu-u\tau_{xx}-v\tau_{xy}+q_x\end{bmatrix},$$

$$\mathbf{G}=\begin{bmatrix}\rho v\\ \rho uv-\tau_{xy}\\ \rho v^2+p-\tau_{yy}\\ Ev+pv-u\tau_{xy}-v\tau_{yy}+q_y\end{bmatrix}. \tag{2}$$

In these equations p is the pressure, ρ is the density, u and v are, respectively, the tangential and normal components of velocity, and E is the total energy defined as $\rho[e+\frac{1}{2}(u^2+v^2)]$, where e is the specific internal energy. These equations are general and can be applied to both continuum and noncontinuum flows. It is only when approximate expressions are substituted for the shearing stress τ_{ij} and heat flux q_j that these equations lose their generality.

Expressions for τ_{ij} and q_j can be obtained from the Boltzmann equation by assuming a molecular velocity distribution function. If this function is written as a series expansion in powers of the Knudsen number (Kn), this approach yields the various conservation equations in successive orders of approximation. The zeroth-order approximation to the distribution function yields the Euler equations, while the first-order expansion yields the Navier–Stokes equations. In 1935, Burnett[14,15] derived the shearing stress tensor and heat flux vector corresponding to the second-order series expansion of the distribution function. The expanded Cartesian components of the shearing stress tensor are

$$\begin{aligned}
\tau_{xx}=&\mu\left(\frac{4}{3}\frac{\partial u}{\partial x}-\frac{2}{3}\frac{\partial v}{\partial y}\right)-K_1\frac{\mu^2}{p}\left[\frac{2}{3}\left(\frac{\partial u}{\partial x}\right)^2+\frac{1}{3}\frac{\partial u}{\partial x}\frac{\partial v}{\partial y}-\frac{1}{3}\left(\frac{\partial v}{\partial y}\right)^2\right]-K_2\frac{\mu^2}{p}\left\{\frac{2}{3}\left[-\frac{\partial}{\partial x}\left(\frac{1}{\rho}\frac{\partial p}{\partial x}\right)\right]-\frac{1}{3}\left[-\frac{\partial}{\partial y}\left(\frac{1}{\rho}\frac{\partial p}{\partial y}\right)\right]-\frac{14}{9}\left(\frac{\partial u}{\partial x}\right)^2\right.\\
&\left.+\frac{7}{9}\left(\frac{\partial v}{\partial y}\right)^2-\frac{2}{3}\frac{\partial u}{\partial y}\frac{\partial v}{\partial x}+\frac{2}{9}\frac{\partial v}{\partial y}\frac{\partial u}{\partial x}+\frac{1}{3}\left(\frac{\partial u}{\partial y}\right)^2-\frac{2}{3}\left(\frac{\partial v}{\partial x}\right)^2\right\}-K_3\frac{\mu^2}{\rho T}\left(\frac{2}{3}\frac{\partial^2 T}{\partial x^2}-\frac{1}{3}\frac{\partial^2 T}{\partial y^2}\right)-K_4\frac{\mu^2}{\rho p T}\left(\frac{2}{3}\frac{\partial p}{\partial x}\frac{\partial T}{\partial x}-\frac{1}{3}\frac{\partial p}{\partial y}\frac{\partial T}{\partial y}\right)\\
&-K_5\frac{\mu^2}{\rho T^2}\left[\frac{2}{3}\left(\frac{\partial T}{\partial x}\right)^2-\frac{1}{3}\left(\frac{\partial T}{\partial y}\right)^2\right]-K_6\frac{\mu^2}{p}\left\{\frac{7}{27}\left(\frac{\partial u}{\partial x}\right)^2-\frac{2}{27}\left(\frac{\partial v}{\partial y}\right)^2-\frac{4}{27}\frac{\partial u}{\partial x}\frac{\partial v}{\partial y}+\frac{1}{12}\left[\left(\frac{\partial u}{\partial y}\right)^2+\left(\frac{\partial v}{\partial x}\right)^2\right]+\frac{1}{6}\frac{\partial u}{\partial y}\frac{\partial v}{\partial x}\right\},\\
\tau_{xy}=&\mu\left(\frac{\partial u}{\partial y}+\frac{\partial v}{\partial x}\right)-K_1\frac{\mu^2}{2p}\left(\frac{\partial u}{\partial x}\frac{\partial u}{\partial y}+\frac{\partial v}{\partial y}\frac{\partial u}{\partial y}+\frac{\partial u}{\partial x}\frac{\partial v}{\partial x}+\frac{\partial v}{\partial y}\frac{\partial v}{\partial x}\right)-K_2\frac{\mu^2}{p}\left\{\frac{1}{2}\left[-\frac{\partial}{\partial x}\left(\frac{1}{\rho}\frac{\partial p}{\partial y}\right)-\frac{\partial}{\partial y}\left(\frac{1}{\rho}\frac{\partial p}{\partial x}\right)\right]-\frac{2}{3}\frac{\partial u}{\partial x}\frac{\partial v}{\partial x}\right.\\
&\left.-\frac{5}{3}\left(\frac{\partial u}{\partial y}\frac{\partial u}{\partial x}+\frac{\partial v}{\partial x}\frac{\partial v}{\partial y}\right)-\frac{2}{3}\frac{\partial v}{\partial y}\frac{\partial u}{\partial y}\right\}-K_3\frac{\mu^2}{\rho T}\frac{\partial^2 T}{\partial x\partial y}-K_4\frac{\mu^2}{2\rho p T}\left(\frac{\partial p}{\partial x}\frac{\partial T}{\partial y}+\frac{\partial p}{\partial y}\frac{\partial T}{\partial x}\right)-K_5\frac{\mu^2}{\rho T^2}\frac{\partial T}{\partial y}\frac{\partial T}{\partial x}\\
&-K_6\frac{\mu^2}{6p}\left(\frac{\partial u}{\partial x}\frac{\partial u}{\partial y}+\frac{\partial u}{\partial x}\frac{\partial v}{\partial x}+\frac{\partial v}{\partial y}\frac{\partial u}{\partial y}+\frac{\partial v}{\partial y}\frac{\partial v}{\partial x}\right),\\
\tau_{yy}=&\mu\left(\frac{4}{3}\frac{\partial v}{\partial y}-\frac{2}{3}\frac{\partial u}{\partial x}\right)-K_1\frac{\mu^2}{p}\left[\frac{2}{3}\left(\frac{\partial v}{\partial y}\right)^2+\frac{1}{3}\frac{\partial u}{\partial x}\frac{\partial v}{\partial y}-\frac{1}{3}\left(\frac{\partial u}{\partial x}\right)^2\right]\\
&-K_2\frac{\mu^2}{p}\left\{\frac{2}{3}\left[-\frac{\partial}{\partial y}\left(\frac{1}{\rho}\frac{\partial p}{\partial y}\right)\right]-\frac{1}{3}\left[-\frac{\partial}{\partial x}\left(\frac{1}{\rho}\frac{\partial p}{\partial x}\right)\right]-\frac{14}{9}\left(\frac{\partial v}{\partial y}\right)^2+\frac{7}{9}\left(\frac{\partial u}{\partial x}\right)^2-\frac{2}{3}\frac{\partial u}{\partial y}\frac{\partial v}{\partial x}-\frac{2}{3}\left(\frac{\partial u}{\partial y}\right)^2+\frac{2}{9}\frac{\partial u}{\partial x}\frac{\partial v}{\partial y}+\frac{1}{3}\left(\frac{\partial v}{\partial x}\right)^2\right\}\\
&-K_3\frac{\mu^2}{\rho T}\left[\frac{2}{3}\left(\frac{\partial^2 T}{\partial y^2}\right)-\frac{1}{3}\left(\frac{\partial^2 T}{\partial x^2}\right)\right]-K_4\frac{\mu^2}{\rho p T}\left(\frac{2}{3}\frac{\partial p}{\partial y}\frac{\partial T}{\partial y}-\frac{1}{3}\frac{\partial p}{\partial x}\frac{\partial T}{\partial x}\right)-K_5\frac{\mu^2}{\rho T^2}\left[\frac{2}{3}\left(\frac{\partial T}{\partial y}\right)^2-\frac{1}{3}\left(\frac{\partial T}{\partial x}\right)^2\right]
\end{aligned} \tag{3}$$

$$-K_6\frac{\mu^2}{p}\left\{\frac{1}{12}\left[\left(\frac{\partial v}{\partial x}\right)^2+\left(\frac{\partial u}{\partial y}\right)^2\right]+\frac{1}{6}\frac{\partial v}{\partial x}\frac{\partial u}{\partial y}-\frac{2}{27}\left(\frac{\partial u}{\partial x}\right)^2+\frac{7}{27}\left(\frac{\partial v}{\partial y}\right)^2-\frac{4}{27}\frac{\partial u}{\partial x}\frac{\partial v}{\partial y}\right\},$$

where μ is the viscosity and T is the temperature. The components of the heat flux vector are

$$q_x=-k\frac{\partial T}{\partial x}+\theta_1\frac{\mu^2}{\rho T}\frac{\partial T}{\partial x}\left(\frac{\partial u}{\partial x}+\frac{\partial v}{\partial y}\right)+\theta_2\frac{\mu^2}{\rho T}\left[\frac{8}{3}\frac{\partial T}{\partial x}\frac{\partial u}{\partial x}+\frac{2}{3}\left(T\frac{\partial^2 u}{\partial x^2}+\frac{\partial T}{\partial x}\frac{\partial v}{\partial y}+T\frac{\partial^2 v}{\partial x\partial y}\right)+2\frac{\partial v}{\partial x}\frac{\partial T}{\partial y}\right]$$
$$+\theta_3\frac{\mu^2}{\rho p}\left[\frac{\partial p}{\partial x}\left(\frac{2}{3}\frac{\partial u}{\partial x}-\frac{1}{3}\frac{\partial v}{\partial y}\right)+\frac{1}{2}\frac{\partial p}{\partial y}\left(\frac{\partial v}{\partial x}+\frac{\partial u}{\partial y}\right)\right]+\theta_4\frac{\mu^2}{\rho}\left(\frac{2}{3}\frac{\partial^2 u}{\partial x^2}+\frac{1}{6}\frac{\partial^2 v}{\partial x\partial y}+\frac{1}{2}\frac{\partial^2 u}{\partial y^2}\right)+\theta_5\frac{\mu^2}{\rho T}\left[\frac{\partial T}{\partial x}\left(\frac{2}{3}\frac{\partial u}{\partial x}-\frac{1}{3}\frac{\partial v}{\partial y}\right)+\frac{1}{2}\frac{\partial T}{\partial y}\left(\frac{\partial v}{\partial x}+\frac{\partial u}{\partial y}\right)\right],$$

(4)

$$q_y=-k\frac{\partial T}{\partial y}+\theta_1\frac{\mu^2}{\rho T}\frac{\partial T}{\partial y}\left(\frac{\partial u}{\partial x}+\frac{\partial v}{\partial y}\right)+\theta_2\frac{\mu^2}{\rho T}\left[\frac{8}{3}\frac{\partial T}{\partial y}\frac{\partial v}{\partial y}+\frac{2}{3}\left(T\frac{\partial^2 v}{\partial y^2}+\frac{\partial T}{\partial y}\frac{\partial u}{\partial x}+T\frac{\partial^2 u}{\partial x\partial y}\right)+2\frac{\partial u}{\partial y}\frac{\partial T}{\partial x}\right]$$
$$+\theta_3\frac{\mu^2}{\rho p}\left[\frac{1}{2}\frac{\partial p}{\partial x}\left(\frac{\partial u}{\partial y}+\frac{\partial v}{\partial x}\right)+\frac{\partial p}{\partial y}\left(\frac{2}{3}\frac{\partial v}{\partial y}-\frac{1}{3}\frac{\partial u}{\partial x}\right)\right]+\theta_4\frac{\mu^2}{\rho}\left(\frac{2}{3}\frac{\partial^2 v}{\partial y^2}+\frac{1}{6}\frac{\partial^2 u}{\partial x\partial y}+\frac{1}{2}\frac{\partial^2 v}{\partial x^2}\right)+\theta_5\frac{\mu^2}{\rho T}\left[\frac{1}{2}\frac{\partial T}{\partial x}\left(\frac{\partial u}{\partial y}+\frac{\partial v}{\partial x}\right)+\frac{\partial T}{\partial y}\left(\frac{2}{3}\frac{\partial v}{\partial y}-\frac{1}{3}\frac{\partial u}{\partial x}\right)\right],$$

where k is the thermal conductivity. The Burnett equations reduce to the Navier–Stokes equations when the second-order terms are neglected. The Burnett equations are valid for flows in which $M^2Kn^2 \ll 1$, where M is the Mach number.[15] Using this strict criterion, their applicability beyond the slip flow regime is questionable.

The constants used in this study for $K_1, K_2, \ldots, K_6$ and $\theta_1, \theta_2, \ldots, \theta_5$ were derived by Burnett and apply to Maxwell molecules, i.e., point centers whose repulsive force varies inversely as the fifth power of distance. These constants are[15]

$$K_1=\frac{4}{3}\left(\frac{7}{2}-\frac{T}{\mu}\frac{d\mu}{dT}\right), \qquad \theta_1=\frac{15}{4}\left(\frac{7}{2}-\frac{T}{\mu}\frac{d\mu}{dT}\right),$$
$$K_2=2, \qquad \theta_2=-45/8,$$
$$K_3=3, \qquad \theta_3=-3,$$
$$K_4=0, \qquad \theta_4=3, \tag{5}$$
$$K_5=3\frac{T}{\mu}\frac{d\mu}{dT}, \qquad \theta_5=3\left(\frac{35}{4}+\frac{T}{\mu}\frac{d\mu}{dT}\right),$$
$$K_6=8.$$

Since Burnett assumed a perfect monatomic gas composed of spherically symmetric molecules, the perfect gas equation of state is applicable and may be written as

$$p=(\gamma-1)\rho e. \tag{6}$$

III. NUMERICAL SOLUTION OF EQUATIONS

A. Finite-difference scheme

In the flow field interior, the Burnett equations are integrated using MacCormack's finite-difference scheme.[16] This is an explicit, predictor-corrector method with second-order accuracy in both space and time. Applying this method to Eq. (1) yields the following difference equations for the first time step:

Predictor:

$$\mathbf{U}_{j,k}^{\overline{n+1}}=\mathbf{U}_{j,k}^{n}-\frac{\Delta t}{\Delta x}(\mathbf{F}_{j+1,k}^{n}-\mathbf{F}_{j,k}^{n})-\frac{\Delta t}{\Delta y}(\mathbf{G}_{j,k+1}^{n}-\mathbf{G}_{j,k}^{n}); \tag{7}$$

Corrector:

$$\mathbf{U}_{j,k}^{n+1}=\frac{1}{2}\left[\mathbf{U}_{j,k}^{n}+\mathbf{U}_{j,k}^{\overline{n+1}}-\frac{\Delta t}{\Delta x}(\mathbf{F}_{j,k}^{\overline{n+1}}-\mathbf{F}_{j-1,k}^{\overline{n+1}})-\frac{\Delta t}{\Delta y}(\mathbf{G}_{j,k}^{\overline{n+1}}-\mathbf{G}_{j,k-1}^{\overline{n+1}})\right], \tag{8}$$

where $\mathbf{F}_{j,k}^{n}=\mathbf{F}(\mathbf{U}_{j,k}^{n})$ and $\mathbf{G}_{j,k}^{n}=\mathbf{G}(\mathbf{U}_{j,k}^{n})$. The subscripts refer to a spatial mesh of points (x_j, y_k) with spacing Δx and Δy (see Fig. 2) and the superscripts refer to times $t=n\Delta t$ where Δt is the time increment. In the above predictor step, $\partial\mathbf{F}/\partial x$ and $\partial\mathbf{G}/\partial y$ are approximated by the forward differences $(\mathbf{F}_{j+1,k}-\mathbf{F}_{j,k})/\Delta x$ and $(\mathbf{G}_{j,k+1}-\mathbf{G}_{j,k})/\Delta y$. In the corrector step they are approximated by the backward differences $(\mathbf{F}_{j,k}-\mathbf{F}_{j-1,k})/\Delta x$ and $(\mathbf{G}_{j,k}-\mathbf{G}_{j,k-1})/\Delta y$. During each succeeding time step, this differencing is reversed in order to eliminate any "biasing" of the solution.

In order to be consistent with the order of the Burnett equations, the derivatives in the shearing stress and heat flux terms appearing in $\mathbf{F}$ and $\mathbf{G}$ are approximated with second-order differences. To reduce computation time, the shearing stress tensor and heat flux vector are computed only at the beginning of each time step.

At the beginning of the computation, freestream flow conditions are specified at each interior grid point. MacCormack's scheme is then used to advance the computation from these initial conditions until the steady-state solution is reached. After each computational step, the flow variables are obtained at each interior grid point from the U vector,

$$\mathbf{U}=\begin{bmatrix}U_1\\U_2\\U_3\\U_4\end{bmatrix}, \tag{9}$$

in the following manner:

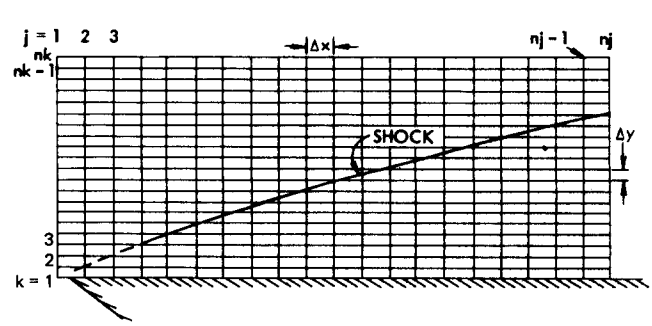

FIG. 2. Computational mesh.

$$\rho = U_1 , \quad u = U_2/U_1 , \quad v = U_3/U_1 ,$$
$$e = U_4/U_1 - (u^2+v^2)/2 , \tag{10}$$
$$p = (\gamma - 1)\rho e , \quad T = p/\rho R .$$

B. Boundary conditions

In the present computational scheme, all flow variables are specified at each boundary grid point. For the grid configuration used in this study, freestream conditions are fixed along the inflow boundary ($j = 1$; $k = 1$, nk) in Fig. 2. Along the top boundary ($j = 2$, $nj - 1$; $k = nk$) the flow variables are obtained by using a zeroth-order extrapolation of the data along the $k = nk - 1$ row. This extrapolation implies that all gradients of flow variables along the top boundary are zero. This is a reasonable assumption since the mesh height is chosen so that the outer edge of the shock does not pass out of the top of the mesh. For conditions along the outflow boundary ($j = nj$; $k = 1, nk$), a first-order extrapolation of interior data is used. For example, the pressures along $j = nj$ are obtained from

$$p_{nj,k} = 2p_{nj-1,k} - p_{nj-2,k} . \tag{11}$$

For mesh points along the flat plate ($j = 2, nj - 1$; $k = 1$), the flow variables are determined by taking into account velocity slip and temperature jump effects. In previous studies,[8–10] the equations used to describe these phenomena were first-order approximations compatible with the order of the Navier–Stokes equations. Schamberg[17] derived the boundary conditions for the Burnett equations using a pertubation series. Although the validity of Schamberg's boundary conditions has been questioned in the past,[18] they appear to be the only boundary conditions that have been derived thus far for the Burnett equations. These boundary conditions may be written in the following form for a two-dimensional flow over a stationary plate:

$$u_s = \frac{\mu}{\rho}\left[a_1(RT)^{1/2}\frac{\partial u}{\partial y} + \tfrac{3}{4}R\frac{\partial T}{\partial x}\right] + \left(\frac{\mu}{\rho}\right)^2\left[-\tfrac{5}{6}RT\left(\frac{\partial^2 u}{\partial y^2} + \frac{\partial^2 v}{\partial x \partial y}\right)\right.$$
$$+ b_1 R\frac{\partial T}{\partial y}\frac{\partial u}{\partial y} - \frac{8}{15}\frac{RT}{\rho}\frac{\partial \rho}{\partial y}\frac{\partial u}{\partial y} - 3a_1R(RT)^{1/2}\frac{\partial^2 T}{\partial x \partial y}$$
$$\left. - \tfrac{3}{2}a_1R\frac{(RT)^{1/2}}{\mu}\left(\frac{\partial T}{\partial x}\frac{\partial \mu}{\partial y} + \frac{\partial T}{\partial y}\frac{\partial \mu}{\partial x}\right)\right] , \tag{12}$$

$$T_s = T_w + \frac{\mu}{\rho}\left[c_1(RT)^{1/2}\frac{\partial T}{\partial y}\right] + \left(\frac{\mu}{\rho}\right)^2\left[e_1T\left(\frac{\partial u}{\partial y}\right)^2 + e_2T(RT)^{1/2}\frac{\partial^2 u}{\partial y \partial x} + e_3T(RT)^{1/2}\left(2\frac{\partial^2 v}{\partial y^2}\right) + \tfrac{1}{6}a_1T(RT)^{1/2}\frac{1}{\rho}\frac{\partial \rho}{\partial x}\frac{\partial u}{\partial y} - \tfrac{1}{2}a_1T(RT)^{1/2}\frac{1}{\mu}\frac{\partial \mu}{\partial x}\frac{\partial u}{\partial y}\right.$$
$$\left. + e_4(RT)^{1/2}\frac{\partial u}{\partial y}\frac{\partial T}{\partial x} + \frac{1}{8}\frac{RT}{\rho}\frac{\partial \rho}{\partial x}\frac{\partial T}{\partial x} + e_6\frac{RT}{\mu}\frac{\partial \mu}{\partial x}\frac{\partial T}{\partial x} + e_6RT\frac{\partial^2 T}{\partial x^2} + e_7R\left(\frac{\partial T}{\partial x}\right)^2 + e_8R\left(\frac{\partial T}{\partial y}\right)^2 - \tfrac{1}{14}RT\frac{\partial^2 T}{\partial y^2} - \frac{1}{14}\frac{RT}{\mu}\frac{\partial \mu}{\partial y}\frac{\partial T}{\partial y}\right] . \tag{13}$$

In these equations, u_s is the slip velocity, T_s is the temperature of the gas at the wall, T_w is the temperature of the wall, and R is the gas constant. The various constants are determined from the following expressions:

$$a_1 = \left(\frac{\pi}{2}\right)^{1/2}\left(\frac{2-\sigma}{\sigma}\right) ,$$
$$b_1 = -5.167 , \quad b_2 = 0.8749 ,$$
$$c_1 = \frac{15}{8}\left(\frac{\pi}{2}\right)^{1/2}\left(\frac{2-\alpha}{\alpha}\right) ,$$
$$e_1 = -\left[0.31655 + \frac{\pi}{8}\left(\frac{2-\sigma}{\sigma}\right)^2 - \frac{\pi}{4}\left(\frac{2-\sigma}{\sigma}\right)\left(\frac{2-\alpha}{\alpha}\right)\right] ,$$
$$e_2 = -\left(\frac{\pi}{2}\right)^{1/2}\left[\frac{1}{4}\left(\frac{2-\alpha}{\alpha}\right) + \frac{1}{2}\left(\frac{2-\sigma}{\sigma}\right)\right] ,$$
$$e_3 = -\frac{1}{2}\left(\frac{\pi}{2}\right)^{1/2}\left(\frac{2-\alpha}{\alpha}\right) , \tag{14}$$
$$e_4 = -\left(\frac{\pi}{2}\right)^{1/2}\left[\frac{33}{8}\left(\frac{2-\alpha}{\alpha}\right) - \frac{1}{4}\left(\frac{2-\sigma}{\sigma}\right)\right] ,$$
$$e_5 = \frac{45}{16}\left(\frac{\pi}{2}\right)^{1/2}\left(\frac{2-\alpha}{\alpha}\right) , \quad e_6 = 107/56 ,$$
$$e_7 = -7.9888 , \quad e_8 = -5.4912 ,$$
$$e_9 = -1.7183 , \quad e_{10} = \frac{159}{16}\left(\frac{\pi}{2}\right)^{1/2}\left(\frac{2-\alpha}{\alpha}\right) ,$$

where α is the accommodation coefficient and σ is the reflection coefficient. For this study, it was assumed that the flow was perfectly diffuse and fully accommodated, i.e., $\sigma = \alpha = 1$. The flow variables along the wall are determined in the following manner:

$$\rho^n_{j,1} = 3\rho^n_{j,2} - 3\rho^n_{j,3} + \rho^n_{j,4} ,$$
$$T^n_{j,1} = T_s , \quad u^n_{j,1} = u_s , \tag{15}$$
$$v^n_{j,1} = 0 , \quad p^n_{j,1} = \rho^n_{j,1}RT^n_{j,1} .$$

For consistency, second-order difference approximations were employed for the various spacial derivatives in the velocity-slip and temperature-jump expressions. Because of the existence of spatial derivatives of temperature in both directions in Eq. (13), a simultaneous set of $nj - 1$ algebraic equations result after the partial derivatives are replaced by differences. These equations can be readily solved, however, since the coefficient matrix is tridiagonal. Further details on the numerical procedures used to implement Schamberg's boundary conditions can be found in Ref. 19.

IV. NUMERICAL RESULTS

The computational method developed in the study to solve the complete Burnett equations has been applied to a leading edge flow field corresponding to an experimental argon test of Becker.[20] The flow conditions are

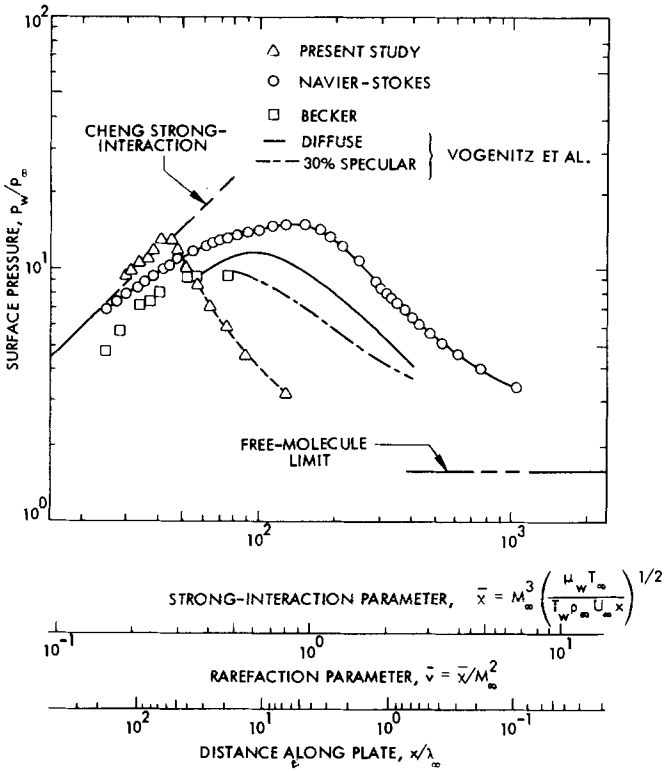

FIG. 3. Comparison of surface pressures.

$$M_\infty = 12.66\,, \qquad p_\infty = 3.73\ \mathrm{N/m^2}\,,$$
$$\mathrm{Pr} = 0.667\,, \qquad T_w/T_t = 0.0835\,,$$
$$\gamma = 1.67\,, \qquad T_\infty = 64.5\ ^\circ\mathrm{K}\,, \tag{16}$$
$$\mathrm{Re}_\infty/L = 93,100/\mathrm{m}\,, \qquad \lambda_\infty = 0.023\ \mathrm{cm}\,,$$

where Pr is the Prandtl number, γ is the ratio of specific heats, Re_∞/L is the freestream Reynolds number per unit length, T_t is the stagnation temperature, and λ_∞ is the mean free path in the freestream. In order to be consistent with the calculations used for comparison, the local viscosity was determined from[21]

$$\mu = 2.27\times10^{-5}(T/300\ ^\circ\mathrm{K})^{0.68}\ [\mathrm{N(sec/m^2)}] \tag{17}$$

and the coefficient of thermal conductivity was calculated from

$$k = [\mu\gamma R/\mathrm{Pr}(\gamma - 1)] \tag{18}$$

by assuming a constant Prandtl number. A computational grid consisting of 21 grid points in both the x and y directions was used to compute this leading edge flow field with $\Delta x = 0.1524$ cm and $\Delta y = 0.06096$ cm.

The computed surface pressures are compared with Becker's experimental data,[20] the Monte Carlo simulation results of Vogenitz *et al.*,[2] and the Navier–Stokes results of Tannehill *et al.*[10] in Fig. 3. The Burnett wall pressures are substantially less than either the Monte Carlo or Navier–Stokes results near the leading edge of the plate. Farther back, near the merged-layer region, the computed pressures rise above the Monte Carlo and Navier–Stokes pressures and asymptotically approach the pressures predicted by the strong-interaction theory of Cheng.[22]

Figure 4 compares the computed slip velocities with the experimental results of Becker and the Navier–Stokes predictions. The computed slip velocities are greater than those obtained in the other studies through all regions up to the strong-interaction zone. Both numerical and experimental results indicate a slip velocity downstream of the merged layer.

Figure 5 compares density profiles at selected positions along the plate with the Navier-Stokes and Monte Carlo results. The computed profiles seem to indicate a weaker over-all shock structure than that predicted in the other studies. The computed peak density at the farthest downstream position is about 26% less than its Navier–Stokes counterpart. The rapid density decrease from plate to freestream values, in the profiles closest to the leading edge, indicates a much broader transition region than that predicted by either the Navier–Stokes or Monte Carlo results.

The variation of the skin friction coefficient,

$$C_f = \frac{\mu_w(\partial u/\partial y)_w}{\frac{1}{2}\rho_\infty U_\infty^2}\,, \tag{19}$$

is shown in Fig. 6, where U_∞ is the freestream velocity. The free-molecule limit is given by

$$(C_f)_{fm} = \left(\frac{2}{\pi\gamma}\right)^{1/2}\frac{\gamma+1}{2\gamma M_\infty} \tag{20}$$

and is indicated in the figure. The skin friction coefficients predicted by the Burnett equations near the leading edge are substantially less than those predicted by the Navier–Stokes equations.

The variation of the coefficient of heat transfer, including the "sliding-friction" term of Maslen,[23]

$$C_h = \frac{[k(\partial T/\partial y)]_w + u_s[(\mu(\partial u/\partial y)]_w}{\rho_\infty U_\infty[\gamma R/(\gamma-1)](T_{t_\infty} - T_w)}\,, \tag{21}$$

is shown in Fig. 7. The coefficients of heat transfer predicted by the Burnett equations near the leading edge are lower than those predicted by the Navier–Stokes equations but rise above the Navier–Stokes results farther downstream.

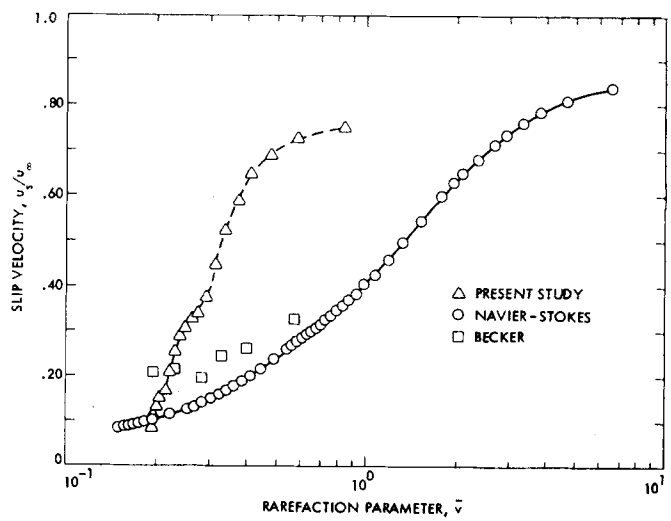

FIG. 4. Comparisons of the surface slip velocities.

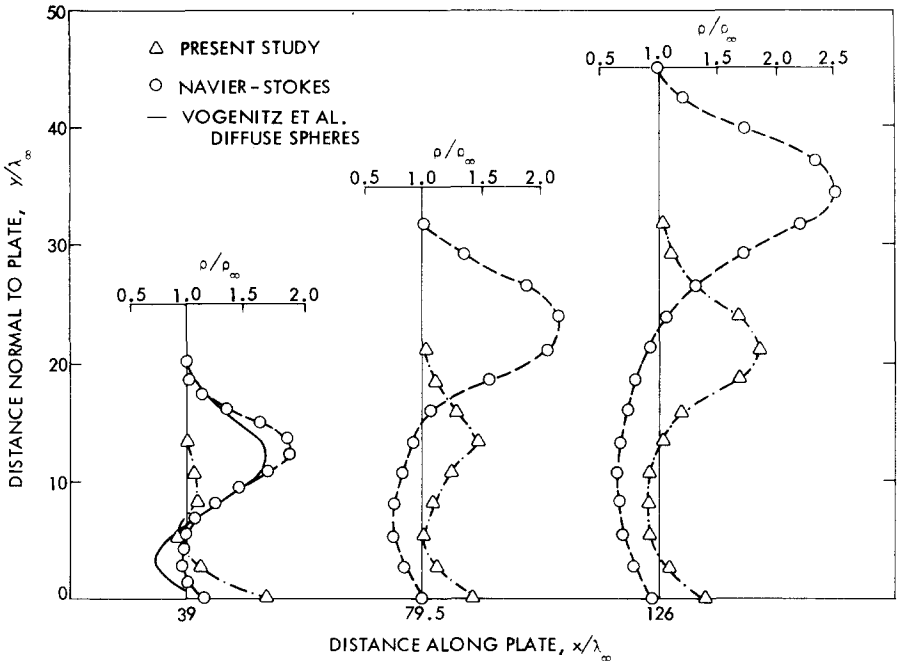

FIG. 5. Shock wave development on plate and density profiles.

V. CONCLUDING REMARKS

In this study, the rarefied flow near the sharp leading edge of a flat plate has been computed using a finite-difference solution of the complete Burnett equations in conjunction with the second-order Schamberg boundary conditions. The region under consideration extends from the leading edge to the strong-interaction regime. The results, presented here for a high-Mach-number rarefied argon case, have been compared with experimental data, a numerical solution of the complete Navier–Stokes equations, and a Monte Carlo simulation. Based on these comparisons, it is evident that the Burnett equations in conjunction with Schamberg's boundary conditions give a much less accurate description of the rarefied flow field near the leading edge than do the Navier–Stokes equations. This result tends to confirm the belief that the Burnett equations cannot be used to progress into rarefied regions where the Navier–Stokes equations are already invalid.

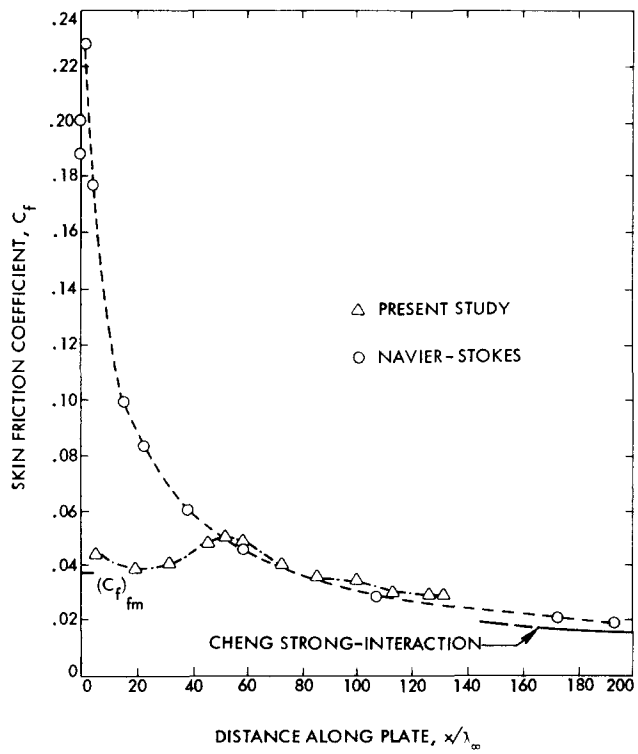

FIG. 6. Skin friction variation along the plate.

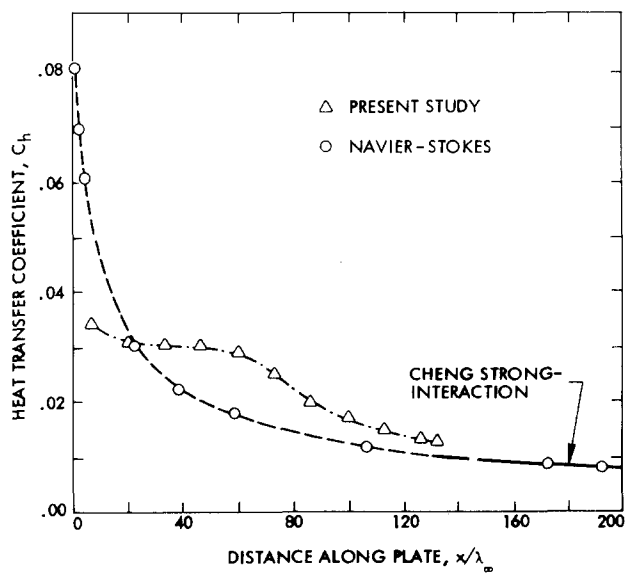

FIG. 7. Conduction and "sliding friction" heat transfer to the wall.

ACKNOWLEDGMENT

This work was supported by the Engineering Research Institute of Iowa State University.

*Present address: Sandia Laboratories, Albuquerque, New Mexico 87115.

[1]W. J. McCroskey, S. M. Bogdonoff, and J. G. McDougall, AIAA J. (Am. Inst. Aeronaut. Astronaut.) **4**, 1580 (1966).
[2]F. W. Vogenitz, J. E. Broadwell, and G. A. Bird, AIAA J. (Am. Inst. Aeronaut. Astronaut.) **8**, 504 (1970).
[3]A. B. Huang, P. F. Hwang, D. P. Giddens, and R. Srinivasan, Phys. Fluids **16**, 814 (1973).
[4]H. Oguchi, in *Rarefied Gas Dynamics*, edited by L. Talbot (Academic, New York, 1961), p. 181.
[5]M. L. Shorenstein and R. F. Probstein, AIAA J. (Am. Inst. Aeronaut. Astronaut.) **6**, 1898 (1968).
[6]S. Rudman and S. G. Rubin, AIAA A. (Am. Inst. Aeronaut. Astronaut.) **6**, 1883 (1968).
[7]H. K. Cheng, S. Y. Chen, R. Mobly, and C. R. Huber, Rand Corporation Memorandum RM-6193-PR (1970).
[8]T. D. Butler, Phys. Fluids **10**, 1205 (1967).
[9]S. I. Cheng and J. H. Chen, Phys. Fluids **17**, 1677 (1974).
[10]J. C. Tannehill, R. A. Mohling, and J. V. Rakich, AIAA J. (Am. Inst. Aeronaut. Astronaut.) **12**, 129 (1974).
[11]K. J. Victoria and G. F. Widhopf, in *Proceedings of the Third International Conference on Numerical Methods in Fluid Mechanics*, edited by H. Cabannes and R. Temam, p. 254 [Lecture Notes in Physics, Vol. 19, Springer, New York, 1973)].
[12]A. C. Jain and V. Adimurthy, AIAA J. (Am. Inst. Aeronaut. Astronaut.) **12**, 342 (1974).
[13]M. N. Kogan, *Rarefied Gas Dynamics* (Plenum, New York, 1969), p. 175.
[14]D. Burnett, Proc. Lond. Math. Soc. **40**, 382 (1935).
[15]T. C. Lin and R. E. Street, NACA TN 2895 (1953).
[16]R. W. MacCormack, in *Proceedings of the Second International Conference on Numerical Methods in Fluid Dynamics*, edited by M. Holt, p. 151 [Lecture Notes in Physics, Vol. 8, (Springer, New York, 1971)].
[17]R. Schamberg, Ph. D. thesis, California Institute of Technology (1947).
[18]S. A. Schaaf and P. L. Chambre, *Fundamentals of Gas Dynamics*, edited by H. W. Emmons (Princeton U. P., Princeton, 1958), p. 717.
[19]G. R. Eisler, M. S. thesis, Iowa State University (1974).
[20]M. Becker, in *Rarefied Gas Dynamics*, edited by L. Trilling and H. Wachman (Academic, New York, 1969), p. 515.
[21]R. A. Matula, J. Heat Transfer **90**, 319 (1968).
[22]H. K. Cheng, J. G. Hall, T. C. Golian, and A. Hertzberg, J. Aerosp. Sci. **28**, 353 (1961).
[23]S. H. Maslen, J. Aeronaut. Sci. **25**, 400 (1958).